The Balloon-v1 Model for Metals With Improved Cyclic Response

Theodore L. Chang[a,*]

[a] *IRIS Adlershof, Humboldt-Universität zu Berlin, Berlin, Germany, 12489.*

Abstract

A versatile constitutive model is proposed for modelling the complex cyclic response of metals. Within the framework of a revised subloading surface theory, the proposed model incorporates a novel isotropic hardening formulation based on the loading reversal information embedded in the normal yield ratio defined in the subloading surface theory. This formulation enables the model to capture a wide range of cyclic phenomena including cyclic hardening/softening, ratcheting, and stress relaxation under cyclic loading. The versatility of the proposed model is demonstrated through numerical examples involving various cyclic loading scenarios, and the results are compared with experimental data from the literature.

Keywords: constitutive modelling, plasticity, metal, ratcheting, cyclic response

1. Introduction

Predicting the constitutive behaviour of metals under cyclic loading poses a persistent difficulty in the field of solid mechanics. Regardless of their crystalline structure, metals exhibit complex mechanical behaviour under repeated loading. These phenomena [1] include the Bauschinger effect, elastic/plastic shakedown, cyclic hardening or softening, and ratcheting. While conventional plasticity theory [see 2] adequately captures monotonic responses, it frequently lacks the fidelity required to predict these cyclic effects. Consequently, classical frameworks have been extended to establish a variety of advanced plasticity models capable of addressing these limitations.

Among these advanced approaches, two–surface formulations — specifically bounding surface theory [3, 4] and subloading surface theory [5–8] — have gained significant prominence. These frameworks have been successfully applied to a wide range of materials, including metals [e.g., 9, 10].

*corresponding author
Email address: tlcfem@gmail.com (Theodore L. Chang)

Despite differences in nomenclature, the two theories share a fundamental basis: both utilise two evolving surfaces within stress space, namely an inner active surface enclosed by an outer bounding surface. In both frameworks, the surfaces undergo isotropic and kinematic hardening, while the evolution of the inner surface is governed by its proximity to the outer boundary. However, the bounding surface theory [3, 10] is conceptually limited by its non-shrinking elastic domain/core, which inhibits the accurate simulation of hysteresis during small one-sided cycles and prevents the guarantee of smooth stiffness continuity at the elastic–plastic transition [11, see §8.2.3]. A potential solution is to shrink the inner surface to a single point [12]. However, this eliminates the possibility of introducing isotropic hardening, leaving all plastic phenomena to be captured solely by kinematic hardening. This is not ideal since *'the physical mechanism of isotropic hardening would be different from that of the kinematic hardening'* [see 8, § 2.5]. In contrast, the subloading surface theory successfully overcomes these issues while providing a more straightforward mathematical framework and a much simpler numerical implementation [13].

Despite these benefits, the capability of subloading surface theory to describe all key cyclic phenomena remains subject to limitations shared by other conventional and non-conventional plasticity models. For example, hysteresis loops intrinsically lead to the accumulation of plastic strain, meaning plastic shakedown (the formation of stable loops) requires that the active loading surface — whether the classical yield surface or subloading surface — has saturated to a fixed size. This requirement stems from the theoretical premise that *'the* (unbounded) *isotropic hardening model suggests that the specimen will 'shake down' to an elastic state'* [1, pg. 103]. This is best

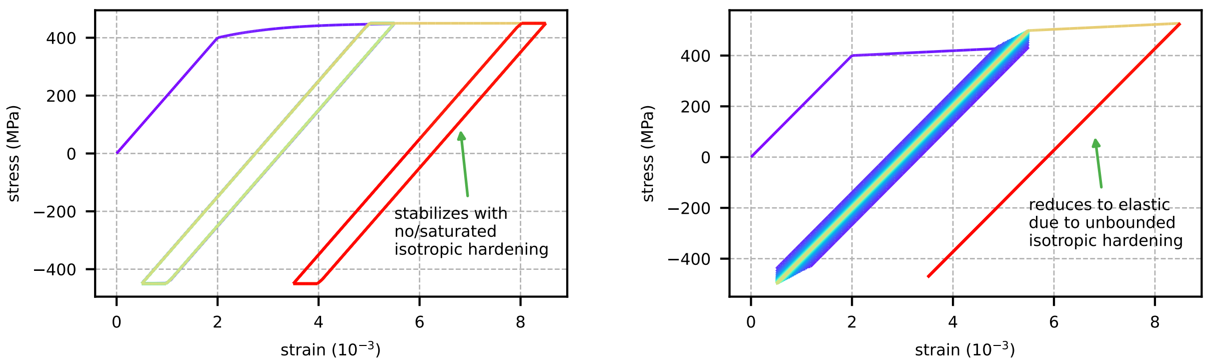

(a) with a bounded isotropic hardening rule

(b) with an unbounded isotropic hardening rule

Figure 1: Conventional isotropic hardening lacks the flexibility to capture complex plastic phenomena

demonstrated by the example depicted in Fig. 1, where the most elementary model [cf. 2, § 1.2.2] is adopted with only isotropic hardening defined. In Fig. 1a, an exponential saturation function (the Voce type) is used for isotropic hardening. Since it is bounded, the hysteresis loop eventually stabilises under cyclic loading with fixed stress amplitudes. Once stabilised, it remains unchanged with further cycling, and all other plastic phenomena (e.g., ratcheting) can only be captured by other mechanisms, such as kinematic hardening. In Fig. 1b, an unbounded linear function is used for isotropic hardening. In this case, the hysteresis loop continues to expand with further cycling, and eventually reduces to an elastic response.

However, experimental observations [e.g., 14–16] consistently show that continued cyclic hardening or softening can occur even after hysteresis loops have stabilised under fixed stress/strain-amplitude cycling. Consequently, reproducing the full range of experimental results [e.g., 17–19] proves extremely challenging, if not impossible, without additional model refinements.

To simulate various cyclic phenomena, a mechanism that conditionally activates or deactivates isotropic hardening (a process also referred to as hardening stagnation or a non-hardening region) must be introduced. Yoshida and Uemori [9, see, § 2.4] introduced an additional *non-isotropic-hardening* surface in the stress space, such that isotropic hardening can be activated or deactivated based on the size of the back stress, and thus the kinematic hardening. One should be aware that this approach does not work if kinematic hardening is not defined, although the absence of kinematic hardening is not practically useful. Although this formulation is effective in certain cases, it still has limitations and cannot capture certain material behaviour [20]. Since the evolution of the back stress is ultimately driven by the plastic strain, such an approach can be equivalently formulated in the strain space. Hashiguchi et al. [7], Ohno [21], Chaboche [22] all adopt a strain space formulation. Such an approach is widely used in the literature as a basic building block for more complex models [see, e.g., 23–25]. Although recent efforts typically incorporate both isotropic and kinematic hardening [e.g., 26], improvements in cyclic response have often relied primarily on increasingly complex kinematic hardening rules [e.g., 27]; see also the review by Kang [28].

In response to these challenges, the present work introduces a novel and efficient constitutive framework. This framework is achieved by incorporating a flexible isotropic hardening rule, grounded in the additive decomposition of plastic strain, with targeted enhancements to the subloading surface theory. The resulting model demonstrates the capability to accurately reproduce a broad spectrum of complex cyclic behaviour, including stable hysteresis loops, cyclic hardening or softening, and the previously intractable phenomenon of work hardening stagnation.

The rest of this paper is organised as follows. In § 2, we briefly summarise the general framework of subloading surface theory. In § 3, the proposed enhancements to the model are presented, including a split of plastic strain based on load reversals, a refined isotropic hardening rule that accounts for contributions from different plastic strain components, and other necessary modifications that further improve the model's flexibility. In § 4, we first demonstrate the model's capabilities through several simple examples, followed by a few more complex cases that simulate experimental results from the literature, demonstrating the effectiveness of the proposed model.

2. Background

To lay the foundation for subsequent discussions, we briefly summarise the general framework of subloading surface theory in this section, primarily following the formulation of Chang [13], which is more concise yet mathematically equivalent to the original by Hashiguchi et al. [7]. It should be noted that the notation system used in this work is *not* fully compatible with that of the previous work [13]. This section does not introduce any new concepts or formulations, which will be presented in the next section.

2.1. Basic Framework

2.1.1. Constitutive Law

Based on the additive decomposition of deformation, conventional elasticity applies. That is, the stress tensor $\boldsymbol{\sigma}$ can be expressed as the double contraction of the elasticity tensor $\boldsymbol{D}_e$ and the elastic strain tensor $\boldsymbol{\varepsilon}^e$,

$$\boldsymbol{\sigma} = \boldsymbol{D}_e : \boldsymbol{\varepsilon}^e = \boldsymbol{D}_e : (\boldsymbol{\varepsilon} - \boldsymbol{\varepsilon}^p)\,, \tag{1}$$

where $\boldsymbol{\varepsilon}$ is the total strain tensor and $\boldsymbol{\varepsilon}^p$ is the plastic strain tensor.

2.1.2. Subloading Surface

The subloading surface differs from the conventional yield surface by an additional scalar field z, ranging from zero to unity, referred to as the normal yield ratio in the existing literature. It can be expressed as

$$f_s = \|\boldsymbol{\eta}\| - zF = \|\boldsymbol{s} - H_\alpha \boldsymbol{\alpha} + (z-1)\, H_d \boldsymbol{d}\| - zF, \tag{2}$$

where $\boldsymbol{\eta}$ is the shifted stress tensor, $\boldsymbol{s} = \boldsymbol{s}(\boldsymbol{\sigma})$ is some measure of the stress tensor $\boldsymbol{\sigma}$, in von Mises models, it is often taken as the deviatoric stress tensor $\boldsymbol{s} = \mathrm{dev}(\boldsymbol{\sigma})$, $\boldsymbol{\alpha}$ is the back stress tensor normalised by H_α, and $\boldsymbol{d}$ is the similarity tensor [13]. Both $\boldsymbol{\alpha}$ and $\boldsymbol{d}$ are internal history variables that evolve in the stress space, with their magnitudes bounded by unity. Those two tensors are further scaled by the scalar fields H_α and H_d respectively, which may also evolve with the development of plasticity. For simplicity, H_α and H_d can be taken as fractions of F, a scalar that characterises the size of the subloading surface and may be interpreted as the (reference) yield stress. Fig. 2 presents a graphical illustration of each term. These two back-stress-like terms have

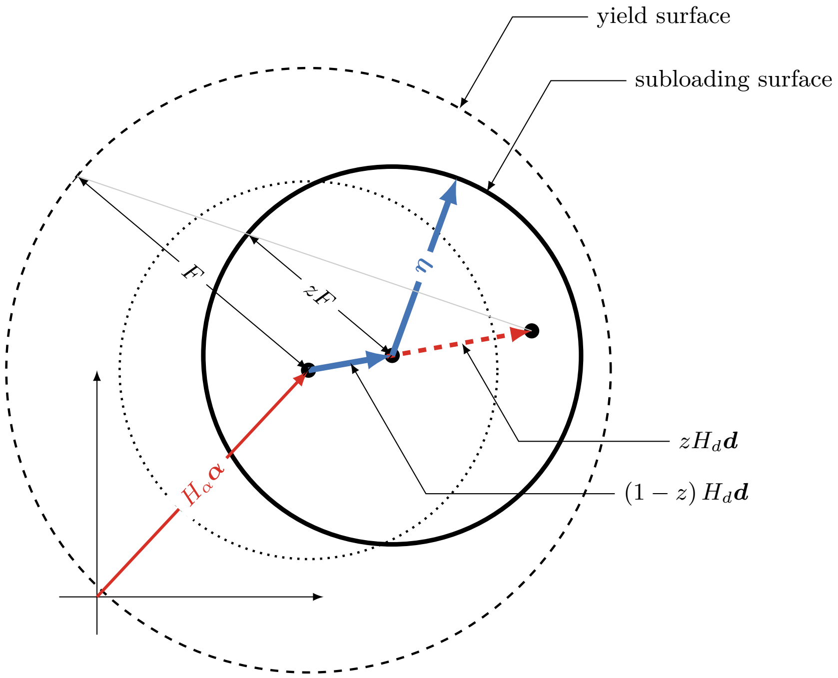

Figure 2: The subloading surface

different effects.

- The first term $H_\alpha \boldsymbol{\alpha}$ is identical to the conventional back-stress term; both $\boldsymbol{\alpha}$ and H_α evolve with the accumulated plastic strain. As commonly understood, this term contributes to kinematic hardening by shifting the centre of the surface and is primarily responsible for the

Bauschinger effect.

- The second term $(1-z)\,H_d\boldsymbol{d}$ has negligible influence during loading as z approaches unity. However, during unloading, as z decreases, the centre of the active plasticity surface is shifted further away from $H_\alpha\boldsymbol{\alpha}$, thereby effectively enhancing the Bauschinger effect. This enables the model to capture the so-called early re-yielding [14]. It also provides a mechanism to control the amount of plastic strain accumulation during one–sided and small loading cycles.

It should be noted that the normal yield ratio z serves a similar purpose to the variable δ in bounding surface formulations [3, 10]. Both variables quantify the proximity of the active plasticity surface to a reference surface, though different terminologies are used in each formulation.

2.1.3. Flow and Evolution Rules

Assuming a von Mises framework (thus $\boldsymbol{s}=\operatorname{dev}(\boldsymbol{\sigma})$) and associative plasticity, the flow rule takes the following form:

$$\dot{\boldsymbol{\varepsilon}^p}=\gamma\dfrac{\partial f_s}{\partial\boldsymbol{\sigma}}=\gamma\dfrac{\partial f_s}{\partial\boldsymbol{\eta}}:\dfrac{\partial\boldsymbol{\eta}}{\partial\boldsymbol{\sigma}}=\gamma\dfrac{\boldsymbol{\eta}}{\|\boldsymbol{\eta}\|}=\gamma\boldsymbol{n}, \tag{3}$$

where γ is the plastic multiplier. The scalar fields are driven by the accumulated plastic strain q, whose rate form is defined as a function of the plastic strain rate $\dot{\boldsymbol{\varepsilon}^p}$. A common choice is to track the magnitude of $\dot{\boldsymbol{\varepsilon}^p}$, thus,

$$\dot{q}=\|\dot{\boldsymbol{\varepsilon}^p}\|=\gamma. \tag{4}$$

For the yield function expressed in Eq. (2), $\dfrac{\partial f_s}{\partial\boldsymbol{\sigma}}$ happens to be normalised. This is not always the case for other yield criteria, where further normalisation may be required to obtain the simplification $\dot{q}=\gamma$.[1] With the above, the following evolution rule is introduced for z,

$$\dot{z}=U\dot{q}, \tag{5}$$

where $U=U(z)$ is a function of z. Furthermore, the scalar bounds $H_\alpha=H_\alpha(q)$, $H_d=H_d(q)$ and $F=F(q)$ are defined as functions of q. It is further required that $H_d<F$ under all circumstances,

[1] Such normalisation is advantageous because the increment $\dot{q}$ does not depend on other tensors, making the computation of derivatives much simpler.

which ensures that the subloading surface is always inside the yield surface. The tensor fields $\boldsymbol{\alpha}$ and $\boldsymbol{d}$ evolve according to Armstrong–Frederick type rules [29], thus,

$$\dot{\boldsymbol{\alpha}} = b_\alpha \left(\boldsymbol{n} - \boldsymbol{\alpha}\right) \dot{q}, \qquad \dot{\boldsymbol{d}} = b_d \left(\boldsymbol{n} - \boldsymbol{d}\right) \dot{q}, \tag{6}$$

where b_α and b_d are material parameters controlling the rate of evolution. For the normalised back stress $\boldsymbol{\alpha}$, alternatively, the linear variant can also be adopted, for example,

$$\dot{\boldsymbol{\alpha}} = b_\alpha \boldsymbol{n} \dot{q}. \tag{7}$$

A combination of both types is also possible [e.g., 30].

3. The `Balloon-v1` Model

In this section, we present a novel isotropic hardening rule based on the framework introduced in § 2, along with other relevant changes, to formulate a versatile constitutive model named the `Balloon`-v1 model.

3.1. History of Load Reversals

In conventional plasticity models, local reversals cannot be easily detected. A common criterion for detecting reversals is the double contraction $\boldsymbol{\eta} : \dot{\boldsymbol{\eta}}$. For example, in the multi-surface theory [31], the exact criterion is used to identify the initiation of a load reversal, which further controls the activation of a new surface.

The normal yield ratio z effectively represents the current 'loading level' at any given moment. By definition, this loading level is normalised between 0 and 1 and thus does not depend on the current size of the yield surface: when it increases, the subloading surface expands, indicating a loading process; when it decreases, the subloading surface contracts, indicating an unloading process. Thus, load reversals can be detected with ease by checking whether z ever decreases within the given (sub-)step.

For a material (point) that has experienced up to N load reversals, let the normal yield ratio at each load reversal be denoted as z_r^j with $j = 1, 2, 3, \cdots, N$ standing for the j-th reversal. The initial value, if required, can be set to zero: $z_r^0 = 0$. We use z_r to denote some measure of the entirety of z_r^j, thus,

$$\boxed{z_r = Z\left(\left\{z_r^j\right\}_{j=0}^{N}\right) = Z\left(z_r^0, z_r^1, z_r^2, \cdots, z_r^N\right).} \tag{8}$$

In the above, $Z(\cdot)$ is a function that maps the collection $\{z_r^j\}_{j=0}^{N}$ to a single scalar z_r. Depending on the specific choice of function Z, z_r embodies different memory effects. For example, z_r can take the maximum/minimum value of the most recent M values. When $M = 1$, z_r is the most recent value z_r^N. When $M \geqslant N$, z_r is simply the maximum/minimum value of all z_r^j. With this ansatz, it is effectively assumed that the material has a limited memory of load reversals. Since by definition z is the ratio between the size of the current subloading surface and that of the yield surface, stress information is inherently embedded in z, thus z_r. This allows one to account for key parameters such as stress magnitude and the mean stress of the cyclic loading protocol, either directly or indirectly. For brevity, we do not explore different possibilities in this work.

3.2. Additive Decomposition of Plastic Strain

It is possible to split the plastic strain $\boldsymbol{\varepsilon}^p$ into at least two parts,

$$\boldsymbol{\varepsilon}^p = \boldsymbol{\varepsilon}^p_m + \boldsymbol{\varepsilon}^p_c + \cdots, \tag{9}$$

with $\boldsymbol{\varepsilon}^p_m$ denoting the 'monotonic' part and $\boldsymbol{\varepsilon}^p_c$ denoting the 'cyclic' part. The rationale behind this split is straightforward: the accumulated plastic strain q defined in Eq. (4) only tracks the total amount of plastic deformation. Although it is non-decreasing, it provides no way to infer further details of the corresponding loading process. As also investigated by Meyer and Ahlström [20], experiments show that q alone '*cannot describe the axial yield stress evolution*' for certain types of metals. The split Eq. (9) allows one to distinguish between the plastic strain accumulated during monotonic loading (according to an appropriate definition of 'monotonic') and that accumulated during load reversals. This distinction makes it possible to account for various microstructural effects, such as the rearrangement/annihilation of dislocations. It is reasonable to assume that the plastic strain increment $\dot{\boldsymbol{\varepsilon}}^p$ within a given (sub-)step would be distributed between two parts according to some rule, which may depend on the current loading level z, and/or its history z_r.

Without loss of generality, one can then define

$$\dot{\boldsymbol{\varepsilon}}^p_m = K_m \dot{\boldsymbol{\varepsilon}}^p, \qquad \dot{\boldsymbol{\varepsilon}}^p_c = K_c \dot{\boldsymbol{\varepsilon}}^p, \tag{10}$$

where $K_m = K_m(z, z_r)$ and $K_c = K_c(z, z_r)$ are functions of z and z_r (or equivalently, $\{z^j_r\}^N_{j=0}$) that yield ratios between zero and unity. It is possible to impose the additional constraint $K_m + K_c = 1$, such that there are exactly two components, $\boldsymbol{\varepsilon}^p = \boldsymbol{\varepsilon}^p_m + \boldsymbol{\varepsilon}^p_c$; however, this is not strictly necessary. A similar split can be applied to q such that

$$\boxed{\dot{q}_m = K_m \dot{q}, \qquad \dot{q}_c = K_c \dot{q}.} \tag{11}$$

It is possible to propose a more sophisticated definition of K_m that may further account for other history variables, such as plastic strain. We refrain from doing so in this work to keep the formulation simple.

3.3. Proposed Isotropic Hardening

With Eq. (11), the isotropic bound F can be defined as a function of both q_m and q_c instead of q alone. Assuming an additive decomposition, it can be expressed as

$$F = F_m + F_c. \tag{12}$$

In the following, we elaborate on the two components, F_m and F_c, and their respective effects on isotropic hardening.

3.3.1. Work/Isotropic Hardening Stagnation

The most distinctive feature of the subloading surface theory is that the normal yield ratio z gradually approaches unity from zero during the loading process. Thus, there is no elastic region during this process, as z accumulates with plastic deformation since it is driven by q as defined in Eq. (5). Eq. (5) can be rearranged and integrated to obtain the change of q due to the change of z, say, for example, from $z = 0$ to some $z = z^* < 1$,

$$\Delta q = \int_0^{z^*} \frac{1}{U}\,\mathrm{d}z. \tag{13}$$

Noting that regardless of the specific form of $U(z)$, the right-hand side is always deterministic (a constant), meaning that loading from $z = 0$ to $z = z^*$ always requires the same amount of plastic strain accumulation Δq.

Due to this deterministic mapping between Δz and Δq, those aforementioned strain space formulations for isotropic hardening stagnation can be equivalently reformulated in the z space, thus the stress space. We assume

$$F_m = F_m(q_m) \tag{14}$$

is a function of q_m solely. By choosing an appropriate K_m, for example, $K_m = 0$ for $0 \leqslant z \leqslant z_r$, it is possible to fully deactivate the evolution of q_m, and thus F_m, during the cyclic loading phase.

This type of stagnation is similar to the approach proposed by Ucak and Tsopelas [32, 33], who used a certain set of criteria based on the same memory surface [21] to distinguish between two distinct regions/phases: the plateau region where isotropic hardening stagnates, and the hardening region where isotropic hardening evolves normally. A recent application of this idea can be found in the work by Hu et al. [34]. Unlike existing formulations, the proposed approach Eq. (14) requires no additional history variables for a secondary surface (whether defined in stress or strain space). Similar information has already been inherently embedded in z. Furthermore, because z is a scalar, it avoids tensor bookkeeping and yields a simpler, more efficient implementation. Finally, because K_m is a continuous function, when z gradually increases, it can be gradually (re-)activated from a partially or fully deactivated state.

3.3.2. Cyclic Hardening/Softening

The cyclic hardening/softening is controlled by F_c, which is assumed to be governed by the following evolution rule,

$$\boxed{\dot{F}_c = b_f\left(H_c - F_c\right)\dot{q}_c \qquad \text{with} \qquad H_c = H_c(q_m).} \tag{15}$$

In the above, b_f is a material parameter that controls the rate of saturation, and H_c is the saturation value that may depend on q_m. It is possible to associate H_c with F_m such that the former is a fraction of the latter. With the evolution of q_c, F_c would gradually saturate to H_c. Meanwhile, since $H_c = H_c(q_m)$ depends on q_m, it would also evolve during monotonic loading phases. Eq. (15)

thus allows multi-stage saturation and cyclic hardening/softening under various loading histories. This differs from other models in the literature [e.g., 21, 25] in which similar saturation can only occur once.

3.3.3. Other Relevant Changes

With Eq. (12), the size of the subloading surface (isotropic hardening) is bounded by $F_m + H_c$ which is governed by q_m solely. Stable hysteresis loops would eventually saturate F to this value via the accumulation of q_c. In principle, a similar definition can be applied to bounds H_α and H_d. However, there is no strong experimental evidence indicating that these bounds exhibit hardening or softening behaviour. To avoid unnecessary complexity, they are defined solely as functions of q_m, i.e., $H_\alpha = H_\alpha\left(q_m\right)$ and $H_d = H_d\left(q_m\right)$.

3.4. Objective Transition

As shown in Eq. (13), for a given interval of z, the corresponding change in q is always constant, regardless of the specific form of $U(z)$ — as long as it is given. However, z only measures the relative loading level. As a result, the response curve becomes steeper when the yield stress is larger, and less so when it is smaller. To make this transition more objective and less dependent on material parameters, we propose the following revision.

$$\boxed{\dot{z} = \frac{U}{F}\dot{q}.} \tag{16}$$

Furthermore, in earlier models [8, 13], the function U does not consider loading history. It is further extended in this work to account for loading history by introducing the dependence on q_m. Thus, $U = U\left(q_m, z\right)$. A typical choice can be

$$U\left(q_m, z\right) = -u \ln z \tag{17}$$

with $u = u\left(q_m\right)$ being a varying parameter that gradually decreases with q_m, rather than a constant. Or, following the suggestion by Chang [13], a power function can be used,

$$U\left(q_m, z\right) = u\left(z^{-n} - 1\right) \qquad \text{for} \qquad 0 < n \leqslant 1, \tag{18}$$

again, with $u = u\left(q_m\right)$.

3.5. *Choice of K_m and K_c*

As explained earlier, the introduction of z_r allows one to identify two distinct loading phases: monotonic loading when z increases from z_r to 1, and cyclic loading when z increases from 0 to z_r. The split functions K_m and K_c should meet the following requirements.

1. For $0 \leqslant z < z_r$, $\dot{q}$ mostly distributes to $\dot{q}_c$.
2. For $z_r \leqslant z \leqslant 1$, $\dot{q}$ mostly distributes to $\dot{q}_m$.
3. The amount of $\dot{q}_m$ accumulated during the cyclic loading phase should be inversely proportional to z_r.

To fulfil these, the following expression is chosen for K_m in this work.

$$K_m = \begin{cases} 0, & 0 \leqslant z < z_r, \\ 1 - \exp \dfrac{z - z_r}{k_r\left(z - 1\right)}, & z_r \leqslant z \leqslant 1, \end{cases} \tag{19}$$

in which k_r is a material parameter that controls the transition. Eq. (19) provides a smooth transition of K_m from zero at $z = z_r$ to unity at $z = 1$. The function is illustrated in Fig. 3. It is

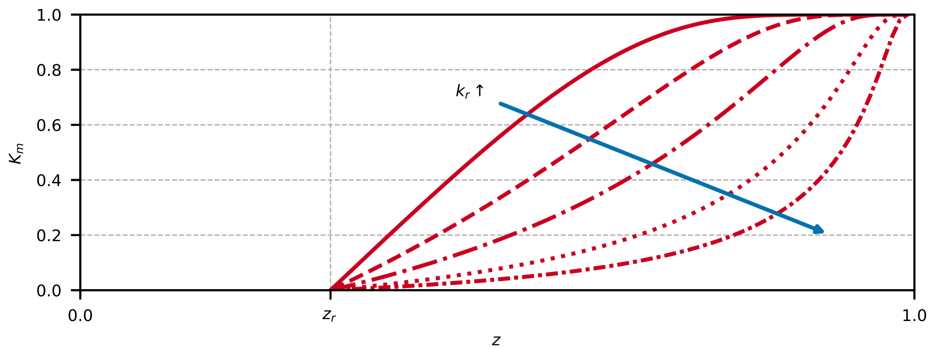

Figure 3: Illustration of K_m defined in Eq. (19)

assumed that $K_c = 1 - K_m$.

3.6. *Summary*

The proposed formulation is summarised in Table 1. It should be emphasised that the formulation presented in this work is general. For specific applications, minor changes, for example, accounting for extra constants $\sqrt{\dfrac{2}{3}}$ in von Mises models [see 13], may be made. For scalar bounds

Table 1: Summary of the proposed formulation

Constitutive Law	$\boldsymbol{\sigma}=\boldsymbol{D}_e:(\boldsymbol{\varepsilon}-\boldsymbol{\varepsilon}^p)$
Subloading Surface	$f_s=\lVert\boldsymbol{\eta}\rVert-zF$
	$F=F_m+F_c$
	$\boldsymbol{\eta}=\boldsymbol{s}-H_\alpha\boldsymbol{\alpha}+(z-1)\,H_d\boldsymbol{d}$
Flow Rule	$\dot{\boldsymbol{\varepsilon}}^p=\gamma\boldsymbol{n}=\gamma\dfrac{\boldsymbol{\eta}}{\lVert\boldsymbol{\eta}\rVert}$
Evolution Rules	$\dot{q}=\gamma$
	$F\dot{z}=U\dot{q}$
	$\dot{q}_m=K_m\dot{q}$
	$\dot{F}_c=b_f\,(H_c-F_c)\,K_c\dot{q}$
	$\dot{\boldsymbol{\alpha}}=b_\alpha\,(\boldsymbol{n}-\boldsymbol{\alpha})\,\dot{q}_m$
	$\dot{\boldsymbol{d}}=b_d\,(\boldsymbol{n}-\boldsymbol{d})\,\dot{q}_m$

$H_\alpha=H_\alpha(q_m)$, $H_d=H_d(q_m)$, $H_c=H_c(q_m)$ and $F_m=F_m(q_m)$, any suitable univariate functions can be chosen, so we keep the corresponding expressions general. Popular options may include a linear component, an exponential component that saturates, and/or a power term. For the 3D formulation, those scalar bounds, along with $\dot{q}$, should be further multiplied by $\sqrt{\dfrac{2}{3}}$ to obtain consistent results.

A careful examination shows that the boundary between subloading surface theory and conventional plasticity is blurred. Specifically, the following can be observed.

1. The term zF controls the effective size of the yield surface: during loading zF grows from 0 to F, so there is no initial elastic domain. It is possible to define a similar loading behaviour in conventional plasticity by using an isotropic hardening function that starts from zero.
2. During unloading, the subloading surface contracts so the current stress point remains on the surface. This can also be achieved in conventional plasticity by simply adjusting isotropic hardening.
3. The term $(1-z)\,H_d\boldsymbol{d}$ acts as an additional, generalised back stress contribution, complementing the conventional $H_\alpha\boldsymbol{\alpha}$ term.

Without introducing any additional (memory) surfaces, Table 1 shows that the subloading surface theory can be regarded as a generalisation of conventional plasticity and is effectively a single-surface theory. The proposed model mimics a balloon, expanding during loading and contracting during unloading. It is thus denoted as the `balloon` model.

3.7. Local System

The overall implementation procedure follows the previous work [13]. Here, we emphasise only the changes introduced by the proposed formulation. The local system consists of two residuals, f_s and z.

$$\boldsymbol{R}=\begin{cases}\|\boldsymbol{\eta}\|-zF,\\[2ex] F\left(z-z_n\right)-U\dot{q}.\end{cases}\tag{20}$$

Taking the local variable as $\boldsymbol{x}=\begin{bmatrix}\gamma & z\end{bmatrix}^\mathrm{T}$, the Jacobian $\boldsymbol{J}$ can be written as

$$\boldsymbol{J}=\begin{bmatrix}\dfrac{\partial\|\boldsymbol{\eta}\|}{\partial\gamma}-z\dfrac{\partial F}{\partial\gamma} & \dfrac{\partial\|\boldsymbol{\eta}\|}{\partial z}-F-z\dfrac{\partial F}{\partial z}\\ \dfrac{\partial F}{\partial\gamma}\left(z-z_n\right)-U\dfrac{\partial\dot{q}}{\partial\gamma}-\dot{q}\dfrac{\partial U}{\partial\gamma} & \dfrac{\partial F}{\partial z}\left(z-z_n\right)+F-\dot{q}\dfrac{\partial U}{\partial z}\end{bmatrix}.\tag{21}$$

In the above, both F and U are functions of both z and γ via q_m and q_c. This differs from the previous formulation [13].

4. Numerical Examples

We present a few numerical examples to demonstrate the capabilities of the proposed model. For brevity, we mostly use normalised quantities in the following examples. Specifically, stresses are normalised by the initial yield stress, which is often the initial size of the conventional yield surface; strains are normalised by the initial yield strain, which is the initial yield stress divided by the elastic modulus. With this normalisation, the conventional yield point is always located at $(1,1)$.

For z_r, the average of the most recent few (2 to 10) z_r^j values is used unless otherwise specified. This choice may appear arbitrary, but it works well in the numerical examples presented here.

It is important to highlight that the following examples are not intended to calibrate the model to match the experimental data perfectly. Rather, the emphasis is on demonstrating the adaptability of the proposed model in qualitatively representing different cyclic behaviour.

4.1. Stiffness Degradation

Fig. 4 demonstrates the gradual degradation of stiffness controlled by u during loading phases where z increases. The following parameters/functions are used.

$$F = F_m = 1, \qquad u = 100 \exp\left(-0.2 q_m\right). \tag{22}$$

Since u effectively controls how fast z increases to unity, a smaller u leads to a slower transition. The proposal in § 3.4 does not rely on an additional history variable, and implementing such degradation is straightforward. Alternatively, it is also possible to associate u with q, in which case such a degradation would occur under cyclic loading as well. In other models, this is typically

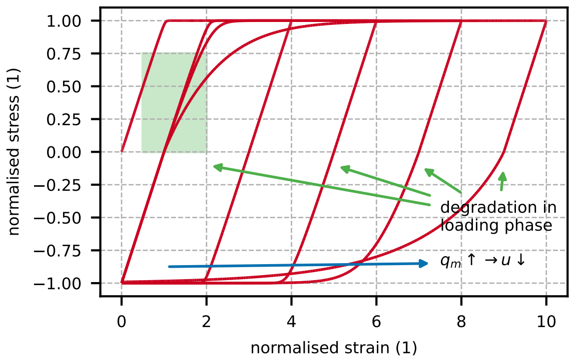

Figure 4: stiffness degradation controlled by u

achieved by introducing a reduction factor for the elastic modulus or by directly turning the elastic modulus itself into a history variable [e.g., 25].

It is also worth noting that H_d is set to zero in this example to highlight the difference between this proposal and other models; hence, unloading phases in which z decreases are similar to those in conventional models and exhibit constant stiffness, namely the initial elastic modulus. For real-world implementations, setting H_d close to F effectively moves the similarity centre towards the boundary, thereby reducing the visual prominence of unloading regions.

4.2. Isotropic Hardening Stagnation

In the example shown in Fig. 5, isotropic hardening is fully deactivated during cyclic loading. As a result, hysteresis loops stabilise immediately. The following configurations are used,

$$k_r = 100, \qquad F = F_m = 1 + 0.05q_m. \tag{23}$$

In terms of z_r, the most recent z_r^j value at load reversal is used.

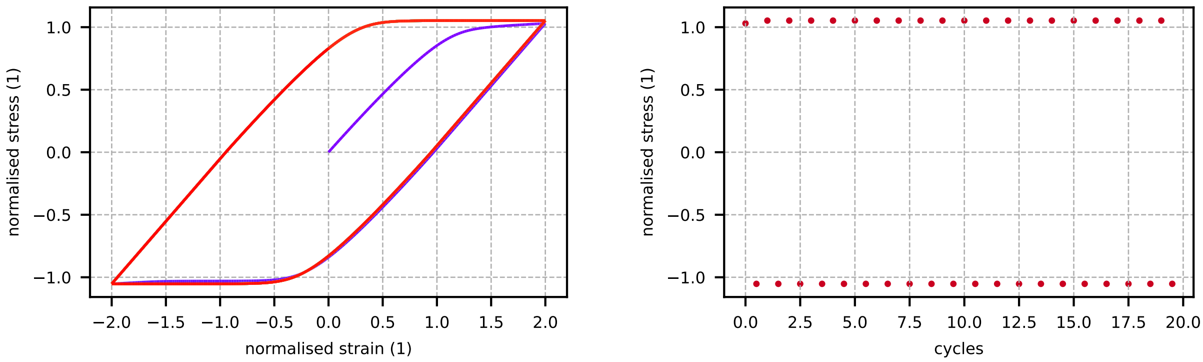

(a) hysteresis response (b) stress amplitude per cycle

Figure 5: isotropic hardening stagnation

If one allows z_r to increase gradually by defining it as the average of a few recent z_r^j values at load reversals, hysteresis loops will stabilise gradually even under cyclic loading with a fixed magnitude of z. This behaviour may vary if z_r is defined differently. Fig. 6 demonstrates such an example by averaging the most recent 8 values.

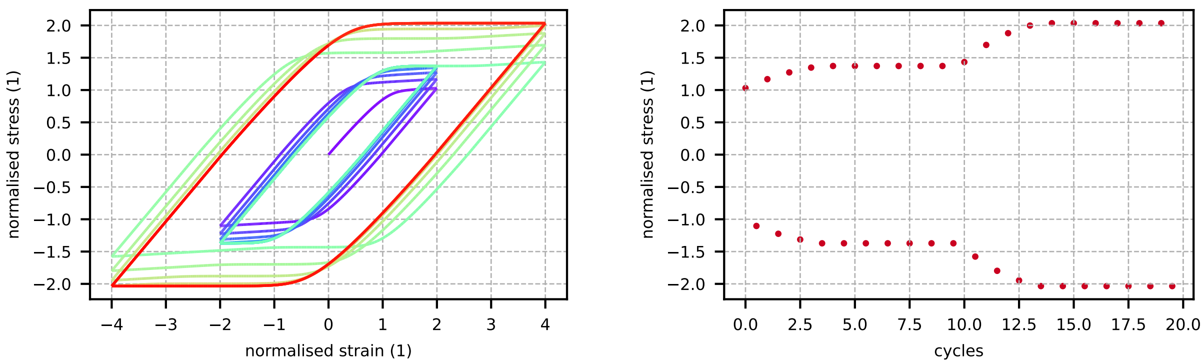

(a) hysteresis response (b) stress amplitude per cycle

Figure 6: Gradual isotropic hardening stagnation

4.3. Cyclic Hardening and Softening

The F_c component is dedicated to modelling cyclic hardening/softening. Fig. 7 shows an example of cyclic hardening using the following expression for H_c.

$$H_c = 0.05 q_m. \tag{24}$$

Since F_c does not evolve when $z < z_r$, the very first cycle thus sets an anchor value. Subsequent loops mostly contribute to q_c, which gradually saturates F_c to H_c. This process repeats whenever a new maximum q_m is reached, and the hysteresis loops eventually stabilise. Since there is no

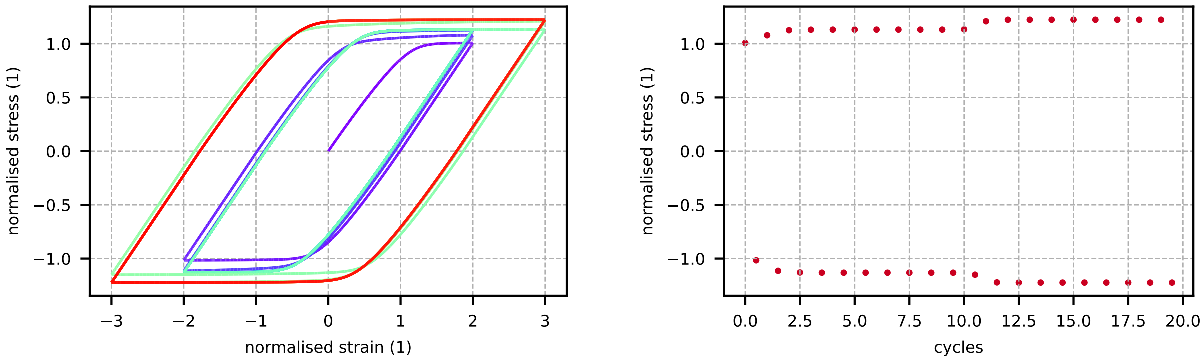

(a) hysteresis response

(b) stress amplitude per cycle

Figure 7: cyclic hardening

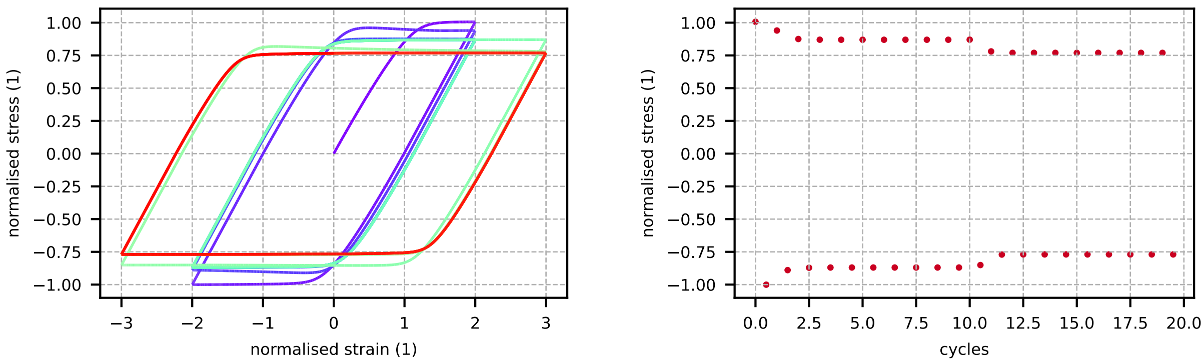

(a) hysteresis response

(b) stress amplitude per cycle

Figure 8: cyclic softening

restriction on how H_c evolves, cyclic softening can be observed if H_c decreases with q_m, as shown in Fig. 8, in which the following expression is used.

$$H_c = -0.05q_m. \tag{25}$$

However, for softening, z_r may stay unchanged after reaching unity, making subsequent softening difficult if not impossible to achieve since Eq. (19) only accounts for the 'relative' load level instead of the absolute one. If z_r has a short memory, e.g., depends on a limited number of recent z_r^j values, it is possible to re-trigger softening by cycling at a relatively lower load level before returning to a higher load level. However, whether such a behaviour is physically meaningful remains to be investigated. It is also possible to refine the definitions of K_m and K_c to account for additional factors, but this is not pursued here for brevity.

4.4. SS304

The parameters and expressions used in this example are summarised in Table 2. SS304 ex-

Table 2: model parameters/expressions for SS304

evolution of z	$u = 200 + 3800 \exp(-2000q_m)$
isotropic hardening F_m	$F_m = 0.2 + 2q_m$ (GPa)
isotropic hardening F_c	$F_c = 0.1 - 0.1 \exp(-100q_m)$ (GPa)
kinematic hardening	linear (Prager type) + exponential (AF type) saturation
similarity	$H_d = 0.8F$

hibits cyclic hardening behaviour that is well captured by a saturating F_c component. Fig. 9 and Fig. 10 show the results of single-step and multistep strain-symmetric cycling, respectively. The

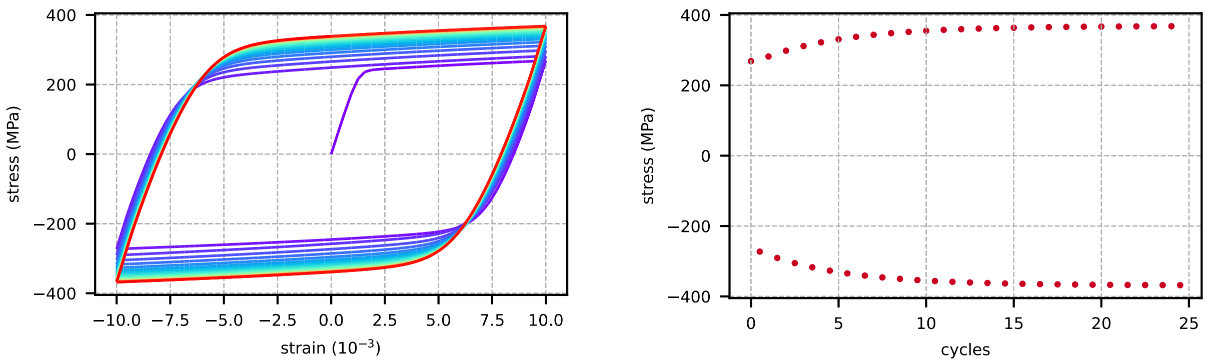

(a) hysteresis response

(b) stress amplitude per cycle

Figure 9: Single-step strain-symmetric cycling of SS304 [cf. 18, Fig. 2]

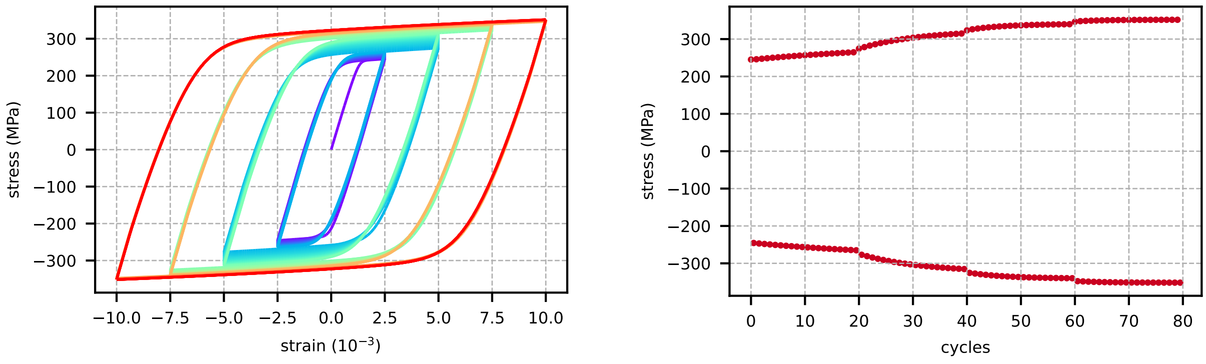

(a) hysteresis response

(b) stress amplitude per cycle

Figure 10: Multistep strain-symmetric cycling of SS304 [cf. 18, Fig. 11]

same set of parameters can also capture satisfactory results for ratcheting under fixed stress/strain amplitude. Fig. 11 shows both cases. Although the model successfully captures the overall characteristics of the experimental data, the initial accumulation of plastic strain (or ratcheting strain) is overestimated relative to the experimental data, as shown in Fig. 11a, indicating that further calibration may be required for improved accuracy.

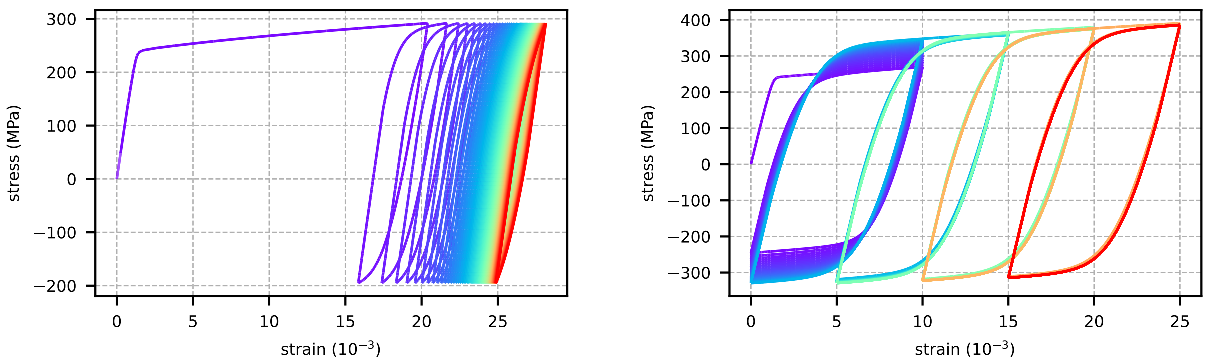

(a) fixed stress amplitude [cf. 18, Fig. 8]

(b) fixed strain amplitude [cf. 18, Fig. 13]

Figure 11: ratcheting of SS304

4.5. CS1018

The parameters and expressions used in this example are summarised in Table 3. The experimental results [18] show a significant correlation between the centre of stabilised hysteresis loops and the plastic history of CS1018. Thus, in this example, the kinematic hardening rule adopts a combination of a linear (Prager-type) component and an exponential (Armstrong–Frederick-type)

Table 3: model parameters/expressions for CS1018

evolution of z	$u = 400 + 3600 \exp(-1000q_m)$
isotropic hardening F_m	$F_m = 0.6 + q_m$ (GPa)
isotropic hardening F_c	$F_c = -0.1 + 0.1 \exp(-100q_m)$ (GPa)
kinematic hardening	linear (Prager type) + exponential (AF type) saturation
similarity	$H_d = 0.8F$

saturation component. By choosing a negative F_c, cycling within a fixed strain range leads to cyclic softening.

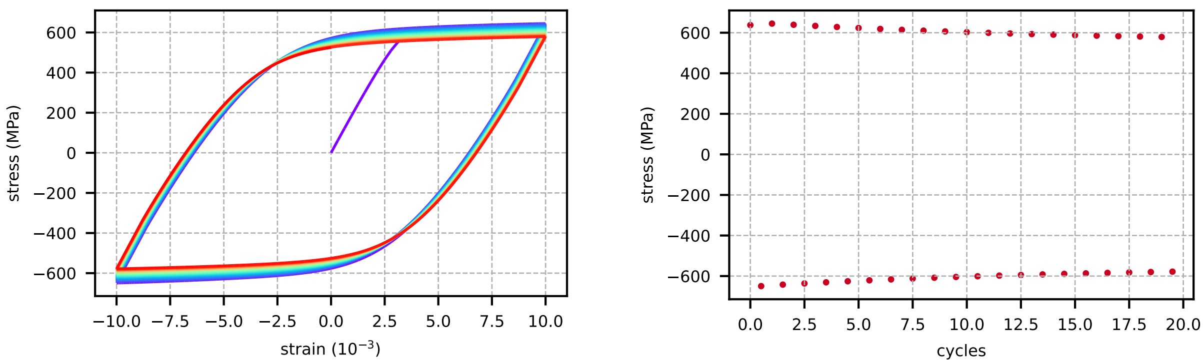

(a) hysteresis response

(b) stress amplitude per cycle

Figure 12: cyclic softening of CS1018 [cf. 18, Fig. 3]

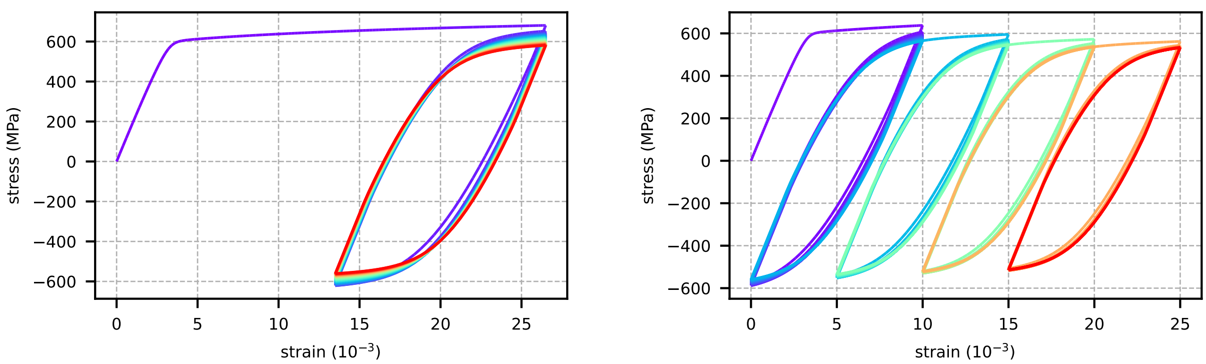

(a) Single-step loading

(b) multistep

Figure 13: Strain-controlled cycling of CS1018 [cf. 18, Figs. 4 and 12]

4.6. Q345

The Q345 steel [see 25, 35] exhibits little to no cyclic hardening/softening. Hysteresis loops stabilise immediately. One can simply set $F_c = 0$. Calibration is relatively straightforward. The parameters and expressions used in this example are summarised in Table 4. Instead of using the

Table 4: model parameters/expressions for Q345

evolution of z	$u = 100 + 3900 \exp\left(-1000q_m\right)$
isotropic hardening F_m	$F_m = 0.33 + q_m$ (GPa)
isotropic hardening F_c	$F_c = 0$ (GPa)
kinematic hardening	linear (Prager type) + exponential (AF type) saturation
similarity	$H_d = 0.8F$

mean of a few recent z values at load reversals, this example uses their maximum. Fig. 14 shows the hysteresis loops under two different loading protocols.

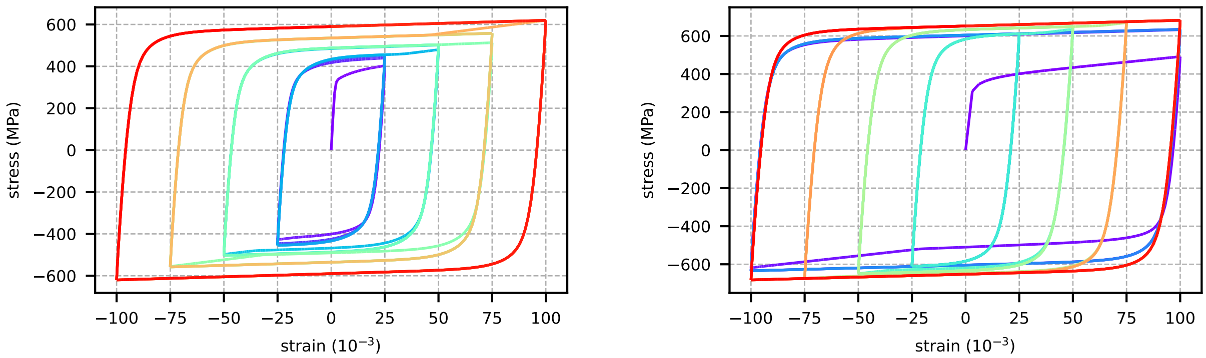

(a) CAA loading protocol

(b) CAA-P1 loading protocol

Figure 14: hysteresis loops of Q345 [cf. 25, Fig. 5]

5. Conclusions

In this work, we introduced the `Balloon-v1` model, a versatile constitutive framework for accurately modelling the complex cyclic response of metallic materials. Built on subloading surface theory, the model achieves its enhanced capabilities without the need for additional, computationally demanding memory surfaces.

The core innovation lies in a novel isotropic hardening formulation that is driven by an additive decomposition of the plastic strain. This split allows the model to distinguish between plastic strain accumulated during monotonic loading and that accumulated during cyclic loading. Leveraging the loading reversal information inherently embedded in the normal yield ratio, z, this framework enables the following key features.

- **Work/Isotropic Hardening Stagnation** By conditionally deactivating the evolution of the monotonic hardening component (F_m) based on the current loading level relative to the history of load reversals (z_r), the model effectively captures the stabilisation of hysteresis loops.
- **Controllable Cyclic Hardening/Softening** The cyclic isotropic hardening component (F_c) is dedicated to modelling this transient behaviour and can saturate in multiple stages, offering a refined response compared with other models in the literature.

The result is a streamlined and efficient formulation that is close to the original subloading surface model. Through a comprehensive set of numerical examples, including simulations of SS304, CS1018, and Q345, we demonstrated its robustness in capturing:

- stable hysteresis loops and stiffness degradation,
- isotropic hardening stagnation,
- cyclic hardening and softening,
- improved ratcheting response.

By providing an alternative to approaches based on increasingly complex kinematic hardening laws, the `Balloon-v1` model offers a powerful and numerically efficient tool for predictive simulations in metal plasticity. Future research will focus on extending the model's application to multiaxial loading conditions and other complex cyclic phenomena such as the multi-stage 'tertiary evolution of ratcheting' [28]. Furthermore, the history of load reversals, as embedded in z_r, only adopts simple functions for the purpose of demonstration in this work. More sophisticated definitions can be explored to account for fatigue-related phenomena in future studies.

Both the uniaxial (1D) and multiaxial (3D) versions of the proposed model are implemented in the open-source finite element analysis framework `suanPan` [36]. All numerical models and the relevant scripts are available in this repository[2].

[2] https://github.com/TLCFEM/balloon-v1

References

[1] S. Suresh, Fatigue of Materials, Cambridge University Press, 1998. doi:10.1017/cbo9780511806575.

[2] J. C. Simo, T. J. R. Hughes, Computational Inelasticity, Springer-Verlag, 1998. doi:10.1007/b98904.

[3] Y. F. Dafalias, E. P. Popov, A model of nonlinearly hardening materials for complex loading, Acta Mechanica 21 (1975) 173–192. doi:10.1007/bf01181053.

[4] R. D. Krieg, A practical two surface plasticity theory, Journal of Applied Mechanics 42 (1975) 641–646. doi:10.1115/1.3423656.

[5] K. Hashiguchi, Constitutive equations of elastoplastic materials with elastic-plastic transition, Journal of Applied Mechanics 47 (1980) 266–272. doi:10.1115/1.3153653.

[6] K. Hashiguchi, Subloading surface model in unconventional plasticity, International Journal of Solids and Structures 25 (1989) 917–945. doi:10.1016/0020-7683(89)90038-3.

[7] K. Hashiguchi, M. Ueno, T. Anjiki, Subloading-overstress model: Unified constitutive equation for elasto-plastic and elasto-viscoplastic deformations under monotonic and cyclic loadings: Research with systematic review, Archives of Computational Methods in Engineering 30 (2023) 2627–2649. doi:10.1007/s11831-022-09880-y.

[8] K. Hashiguchi, Y. Yamakawa, T. Anjiki, M. Ueno, Comprehensive review of subloading surface model: Governing law of irreversible mechanical phenomena of solids, Archives of Computational Methods in Engineering 31 (2024) 1579–1609. doi:10.1007/s11831-023-10022-1.

[9] F. Yoshida, T. Uemori, A model of large-strain cyclic plasticity describing the bauschinger effect and workhardening stagnation, International Journal of Plasticity 18 (2002) 661–686. doi:10.1016/s0749-6419(01)00050-x.

[10] M. Mahan, Y. F. Dafalias, M. Taiebat, Y. Heo, S. K. Kunnath, Sanisteel: Simple anisotropic steel plasticity model, Journal of Structural Engineering 137 (2011) 185–194. doi:10.1061/(asce)st.1943-541x.0000297.

[11] K. Hashiguchi, Foundations of Elastoplasticity: Subloading Surface Model, 3rd ed., Springer International Publishing, 2017. doi:10.1007/978-3-319-48821-9.

[12] Y. F. Dafalias, E. P. Popov, Cyclic loading for materials with a vanishing elastic region, Nuclear Engineering and Design 41 (1977) 293–302. doi:10.1016/0029-5493(77)90117-0.

[13] T. L. Chang, On the subloading surface model for metals: some insights and an efficient numerical implementation, Acta Mechanica 236 (2025) 3695–3717. doi:10.1007/s00707-025-04339-0.

[14] F. Yoshida, T. Uemori, K. Fujiwara, Elastic–plastic behavior of steel sheets under in-plane cyclic tension–compression at large strain, International Journal of Plasticity 18 (2002) 633–659. doi:10.1016/s0749-6419(01)00049-3.

[15] G. Kang, Q. Gao, L. Cai, Y. Sun, Experimental study on uniaxial and nonproportionally multiaxial ratcheting of ss304 stainless steel at room and high temperatures, Nuclear Engineering and Design 216 (2002) 13–26. doi:10.1016/s0029-5493(02)00062-6.

[16] G. Kang, Q. Kan, J. Zhang, Y. Sun, Time-dependent ratchetting experiments of ss304 stainless steel, International Journal of Plasticity 22 (2006) 858–894. doi:10.1016/j.ijplas.2005.05.006.

[17] T. Hassan, S. Kyriakides, Ratcheting in cyclic plasticity, part i: Uniaxial behavior, International Journal of Plasticity 8 (1992) 91–116. doi:10.1016/0749-6419(92)90040-j.

[18] T. Hassan, S. Kyriakides, Ratcheting of cyclically hardening and softening materials: I. uniaxial behavior, International Journal of Plasticity 10 (1994) 149–184. doi:10.1016/0749-6419(94)90033-7.

[19] T. Hassan, L. Taleb, S. Krishna, Influence of non-proportional loading on ratcheting responses and simulations by two recent cyclic plasticity models, International Journal of Plasticity 24 (2008) 1863–1889. doi:10.1016/j.ijplas.2008.04.008.

[20] K. A. Meyer, J. Ahlström, The role of accumulated plasticity on yield surface evolution in pearlitic steel, Mechanics of Materials 179 (2023) 104582. doi:10.1016/j.mechmat.2023.104582.

[21] N. Ohno, A constitutive model of cyclic plasticity with a nonhardening strain region, Journal of Applied Mechanics 49 (1982) 721–727. doi:10.1115/1.3162603.

[22] J. Chaboche, A review of some plasticity and viscoplasticity constitutive theories, International Journal of Plasticity 24 (2008) 1642–1693. doi:10.1016/j.ijplas.2008.03.009.

[23] L. Xu, X. Nie, J. Fan, M. Tao, R. Ding, Cyclic hardening and softening behavior of the low yield point steel bly160: Experimental response and constitutive modeling, International Journal of Plasticity 78 (2016) 44–63. doi:10.1016/j.ijplas.2015.10.009.

[24] Z. Xie, A. Kanvinde, Y. Chen, A constitutive model for various structural steels considering shared hysteretic behaviors, Journal of Constructional Steel Research 176 (2021) 106421. doi:10.1016/j.jcsr.2020.106421.

[25] S. Zheng, R. Zhang, A novel constitutive model under various cyclic loading protocols with large strain ranges considering strain memory effect and loading history dependence, International Journal of Fatigue 202 (2026) 109239. doi:10.1016/j.ijfatigue.2025.109239.

[26] Q. Yang, W. Zhang, Y. Guo, F. Liang, P. Yin, L. Chang, C. Zhou, A universal constitutive model considering strain range dependence effect and transient behaviour for both cyclic softening and hardening steels, Engineering Fracture Mechanics 290 (2023) 109481. doi:10.1016/j.engfracmech.2023.109481.

[27] N. Ohno, J.-D. Wang, Kinematic hardening rules with critical state of dynamic recovery, part i: formulation and basic features for ratchetting behavior, International Journal of Plasticity 9 (1993) 375–390. doi:10.1016/0749-6419(93)90042-o.

[28] G. Kang, Ratchetting: Recent progresses in phenomenon observation, constitutive modeling and application, International Journal of Fatigue 30 (2008) 1448–1472. doi:10.1016/j.ijfatigue.2007.10.002.

[29] C. O. Frederick, P. J. Armstrong, A mathematical representation of the multiaxial bauschinger effect, Materials at High Temperatures 24 (2007) 1–26. doi:10.3184/096034007x207589.

[30] F. Yoshida, A constitutive model of cyclic plasticity, International Journal of Plasticity 16 (2000) 359–380. doi:10.1016/s0749-6419(99)00058-3.

[31] A. S. Semenov, B. E. Melnikov, Multisurface Theory of Plasticity with One Active Surface: Basic Relations, Experimental Validation and Microstructural Motivation, Springer International Publishing, 2022, pp. 207–232. doi:10.1007/978-3-030-97675-0_8.

[32] A. Ucak, P. Tsopelas, Constitutive model for cyclic response of structural steels with yield plateau, Journal of Structural Engineering 137 (2011) 195–206. doi:10.1061/(asce)st.1943-541x.0000287.

[33] A. Ucak, P. Tsopelas, Accurate modeling of the cyclic response of structural components constructed of steel with yield plateau, Engineering Structures 35 (2012) 272–280. doi:10.1016/j.engstruct.2011.10.015.

[34] F. Hu, G. Shi, Y. Shi, Constitutive model for full-range elasto-plastic behavior of structural steels with yield plateau: Formulation and implementation, Engineering Structures 171 (2018) 1059–1070. doi:10.1016/j.engstruct.2016.02.037.

[35] Z. Xie, Y. Chen, Experimental and modeling study of uniaxial cyclic behaviors of structural steel under ascending/descending strain amplitude-controlled loading, Construction and Building Materials 278 (2021) 122276. doi:10.1016/j.conbuildmat.2021.122276.

[36] T. L. Chang, suanpan — an open source, parallel and heterogeneous finite element analysis framework, 2024. doi:10.5281/ZENODO.13820988.